PCCP

Cyclic (Alkyl)(amino)carbenes in Organic and Organometallic Methane C–H Activation: a DFT and MCSCF Study

Journal:	*Physical Chemistry Chemical Physics*
Manuscript ID	CP-ART-08-2020-004080.R1
Article Type:	Paper
Date Submitted by the Author:	27-Sep-2020
Complete List of Authors:	Sun, Zhicheng; University of North Texas, Cundari, Thomas; University of North Texas, Chemistry

Cyclic (Alkyl)(amino)carbenes in Organic and Organometallic Methane C–H Activation: a DFT and MCSCF Study

Zhicheng Sun, Thomas R. Cundari*

Univ. of North Texas, Dept. of Chemistry, Center for Advanced Computing and Modeling (CASCaM), 1155 Union Circle #305070, Denton, Texas 76203

Density functional theory (DFT) and multi-configurational self-consistent field (MCSCF) calculations are used to investigate the electronic and steric properties of cyclic (alkyl)(amino)carbenes (CAACs). Calculations show CAACs' diverse electronic characteristics in terms of its donor and acceptor capabilities. Reactions of CAACs in methane C–H bond activation via insertion and also as a supporting ligand (L) for L(Cp)M (M = Co, Rh, Ir) motifs via C–H oxidative addition are studied. The binding energies and buried volumes are calculated for selected CAACs as ancillary ligands to the L(Cp)Rh motif. Overall, CAACs show highly tunable electronic and steric properties by adjusting their substituents and backbones. Although CAAC may not be viable in activating inert small molecules with low polarity like methane, this class of ligand has great potential as ancillary ligands for transition metal complexes in catalysis. Calculation of C–H activation by L(Cp)Ir and L(Cp)Rh with CAACs as supporting ligands show CAACs can render the reaction more amenable to catalysis by destabilizing the oxidative addition products while keeping the reaction mildly exergonic, and the barriers reasonable.

Introduction

Alkanes are a major component of natural gas and crude oil. However, C–H activation of light alkanes remains a challenge due to the strong sp^3 C–H bonds of the former.[1-7] Very harsh reaction conditions involving high temperatures are utilized in industry.[8] In the 1980s, Bergman,[9-13] Jones,[14-16] Graham,[17,18] and their co-workers showed that L(Cp^*)M complexes ($Cp^* = \eta^5$-$C_5(Me)_5$; M = Rh, Ir; L = CO, PMe_3) have the ability to activate saturated hydrocarbons via oxidative addition (OA). OA was directly observed by Janowicz and Bergman via photogeneration of $Cp^*Ir(PMe_3)$ and reaction with the alkane solvent, RH, to give $Cp^*Ir(R)(H)(PMe_3)$.[10] Then $Cp^*Ir(R)(H)(PMe_3)$ thermally eliminates RH under methane to give very stable $Cp^*Ir(Me)(H)(PMe_3)$.[10] Some computational studies have reported the electronic structures of the activating complexes and the reaction mechanisms.[19-22] The extensive study on the L(Cp^*)M system and the isolation of C–H activation products paved the way for more experimental and computational studies on C–H activation and functionalization with organometallic compounds. Depending on the choice of the transition metal and ancillary ligands, different M/L combinations can show drastically different reaction kinetics, thermodynamics and even different mechanistic pathways for C–H activation.

Successful synthesis and characterization of phosphinocarbenes by Bertrand and co-workers[23] and N-heterocyclic carbenes (NHCs) by Arduengo *et al.*[24] have inspired chemists to study carbenes as supporting ligands in transition metal complexes. NHC ligands have shown their capabilities in organometallic catalysis,[25-27] including intermolecular and intramolecular C–H activation.[28,29] Another family of stable carbenes, cyclic alkyl(amino)carbenes, CAACs, have attracted increasing attention in coordination chemistry and transition metal catalysis as supporting ligands.[30-32] When the σ-withdrawing and π-donating nitrogen in NHC is replaced by a σ-donating alkyl group in CAAC, the σ-donating and the π-accepting ability of the carbene increases, as evidenced by a higher energy HOMO and a lower energy LUMO, respectively. The strong π-accepting ability of CAAC ligands better stabilizes electron-rich, late transition metal complexes with lower coordination numbers, which in turn could make open coordination sites more accessible for metal-centered C–H coordination and activation. Formation of a σ-alkane complex before oxidative addition permits π-backdonation from a filled metal d orbital to the σ* orbital of a methane C–H bond, which should facilitate homolytic cleavage of the C–H bond.[33,34] However, catalysis with CAAC-supported coordination compounds is still in its infancy. In addition to the large research effort made to study the organometallic chemistry of CAACs, isolated stable singlet ligands have the ability to mimic transition metals and activate small, inert molecules as well.[35,36] The smaller singlet-triplet gap and the stronger electrophilicity and nucleophilicity may make CAACs good candidates as organocatalysts for activating very enthalpically strong bonds. The Bertrand group has demonstrated CAACs' ability to activate H_2,[37] B–H,[38,39] Si–H,[38,40] P–H,[38] and N–H bonds.[37]

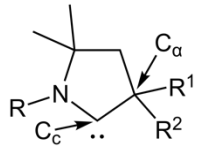

Figure 1. Representation of a five-membered ring CAAC. In this paper, the carbon attached to the carbene carbon (C_c) is defined as C_α, and the two substituents on the C_α are defined as R^1 and R^2.

The first focus of this research is to study CAACs' ability to serve as an organocatalyst in methane C–H activation. The second focus of this research is to discover the effect of different CAACs as supporting ligands on the performance of transition metal complexes of the type L(Cp)M (M = Group 9 metal, L = neutral, $2e^-$ donor) for methane C–H activation, and to offer insight into compound electronic structure, mechanisms and catalyst design. NHC ligands have demonstrated their electronic and steric tunability.[41-45] Structural data have been used to evaluate the extent of σ- and π-bonding in some complexes. Computational descriptors such as Tolman cone angle and buried volume calculated from X-ray structures of transition metal phosphine and NHC complexes, respectively, provided more insight to ligands' steric properties.[46] NHCs have also proved their value as ligands for replacing tertiary phosphine ligand to support transition metals in organometallic catalysis, notably in Grubbs' catalysts for olefin metathesis.[47-50] But compared to the well-studied NHC ligands, the tunability of CAAC ligand is less characterized. Due to the synthetic availability of CAACs at the current time, some of the CAACs in this computational research are "hypothetical." However, according to the synthetic routes reported by Bertrand *et al.*, the choice of R^1 and R^2 is seemingly unlimited, except for H, and aryl groups seem best tolerated as substituents on the nitrogen center (R), **Figure 1**.[31] This research seeks to provide a better understanding of CAAC reactivities and properties from a computational perspective by replacing the traditional carbonyl and phosphine ligands on the classic L(Cp^*)M complexes by Bergman,[1-5] Jones,[6-8] and Graham.[9,10] The structure and bonding of transition metal carbene complexes supported by CAAC, each decorated with different substituents, ligated to Group 9 transition metals (Co, Rh and Ir) will be compared and contrasted. We will compare activation energies of complexes of the same Group 9 metal but with different substituents on CAAC supporting ligands and examine how barriers change with respect to the steric and electronic properties of different CAACs. The mechanism for this catalytic reaction step will be modelled as an OA.

Computational methods

Density functional theory (DFT) calculations via Gaussian 16[51] was used for describing all the molecules utilizing the hybrid meta-GGA functional, ωB97XD[52]. The effective core potential (ECP) basis set def2-SVP[53] was used for the metal and 6-31G(d) for other atoms for geometric optimization and frequency calculations. Geometries were optimized without symmetry constraint. Harmonic vibrational frequencies confirm the nature of intermediates (no imaginary frequency) and transition states (only one imaginary frequency). Single point calculations were done with the larger def2-TZVP[53] basis set for metal atoms and 6-311++G(d,p) for other atoms. All Gibbs free energies and thermal corrections for optimized structure were determined at 298.15 K and 1 atm pressure. The methane C–H activation by

Wasserman *et al.* was studied experimentally in the gas phase, so for simplicity it was decided to model CAAC's impact as an ancillary ligand in the gas phase as well.[11]

The GAMESS[54] package was used for multi-configurational self-consistent field (MCSCF) calculations to study the frontier orbitals of the CAAC ligands and (CAAC)(Cp)M motifs. Optimized structures from DFT calculations were used as geometries for CASSCF (CAS = complete active space) single-point calculations. CASSCF calculations were started from small active spaces (electrons, orbitals) (2,2) and proceeded to the largest (12,12) active spaces. Natural orbital occupation numbers (NOON) and the natural orbital (NO) plots were studied to assess the suitability of various active space selections. The results and discussion for CAAC ligands in this paper are based on CAS(8,8)/6-31G(d) calculations after careful analysis of NO from among all the active spaces studied. 6-31G basis is used for H atoms. CAS(12,12) active space was chosen for the (CAAC)(Cp)M motifs and SBKJC ECP basis was used for the metal atoms.

Results and discussion

The discussion of the calculational results will be divided into three subsections. In the first section, the electronic structures of different CAAC ancillary ligands will be analyzed. In the second section, results of different CAAC ligands activating methane will be compared and contrasted to those presented in the experimental study reported by the Turner group.[55] In the third section, methane C–H activation computational results of (CAAC)(Cp)M with three different metals (Co, Rh, and Ir) will be compared to carbonyl- or trimethylphosphine-supported (Cp)M complexes inspired by the work of Bergman,[9-13] Jones,[14-16] and Graham.[17,18] and their co-workers.

1. CAAC Ligands: Structure and Reactivity

Phukan *et al.* reported a very extensive study on a wide selection of five-membered CAACs with different substituents, focusing on geometries, ligand properties, and activation of H–H and N–H bonds of dihydrogen and ammonia.[56] The CAAC ligands studied in this project are shown in **Figure 2** along with the DFT-calculated HOMO and LUMO orbital energies (eV). Five-membered CAACs with bulkier substituents like cyclohexane (**2**) and 2,6-diisopropylphenyl (Dipp) (**3**) were studied along with two diamino-CAACs with saturated (**4**) and unsaturated (**5**) backbones. A member of the newly synthesized class of 6-membered CAACs[57] (**6**) and an NHC (**7**) were also represented.

a.

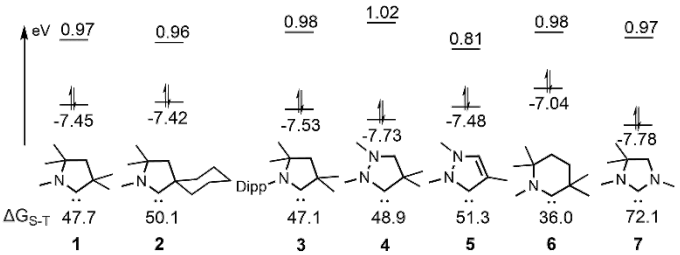

Figure 2. ωB97XD/6-311++G(d,p) calculated HOMO-LUMO energies (eV) and the free energy difference between singlet and triplet states (ΔG_{S-T}) of the carbenes studied.

1.1. Optimized Molecular Structures

	C_c–N (Å)	C_c–C_α (Å)	∠N–C_c–C_α (°)
1 singlet	1.32	1.53	106.0
1 triplet	1.39	1.50	114.7
2 singlet	1.31	1.52	105.7
2 triplet	1.38	1.51	116.4
3 singlet	1.32	1.53	106.5
3 triplet	1.39	1.50	116.1
4 singlet	1.30	1.53	105.3
4 triplet	1.38	1.51	115.5
5 singlet	1.34	1.45	102.6
5 triplet	1.40	1.39	113.7
6 singlet	1.32	1.52	117.6
6 triplet	1.38	1.50	121.2

Table 1. Unrestricted **ω**B97XD/6-31G(d) calculated bond lengths and N–C_c–C_α bond angles of singlet and triplet states of CAAC ligands 1 **-** 6**.**

The key parameters of DFT-optimized CAAC structures **1** – **6** are collected in **Table 1**. Triplet CAACs show longer (~0.07 Å) C_c–N bond lengths and slightly shorter C_c–C_α bond lengths (~0.02 - 0.03 Å) than the corresponding singlets. It is further noted that the optimized structures of CAACs possess nonplanar structures, which is expected due to the presence of multiple sp^3 hybridized carbons (except for **5**). Singlet CAACs are more planar than triplet CAACs. This could be due to the triplet CAACs being better in forming hybridized orbitals, which can be seen from the elongated C_c–N bonds (by 0.06 to 0.08 Å) in triplets while the change in C_c–C_α lengths are much smaller (0.01 to 0.03 Å, except for **5** due to the unsaturation). Introducing a bulky cyclohexane substituent in **2** at the C_α attached to the C_c shortens both C_c–N and C_c–C_α very slightly, by 0.01 Å. Changing the alkyl group to a bulky aryl group on the amino N in **3** changes the geometry very little. Finally, changing the sp^3 carbon to a second amino group shortens C_c–N by 0.02 Å (**4**), **Table 1**. For NHC **7** singlet, both amino nitrogens have sp^2 hybridization, which means the N lone pairs locate on the p_z orbitals. Both C_c–N bonds are 1.38 Å. One of the N of **7** triplet state is sp^3 hybridized. The C_c–N(sp^2) and C_c–N(sp^3) bonds are 1.41 and 1.38 Å, respectively.

1.2. Electronic Structure

By changing the substituents on the alpha carbon (C_α), particularly that attached to the carbene carbon (C_c), very different electronic and steric profiles can be obtained. The steric parameters of CAAC **1** - **6** and PMe_3 were characterized with Samb*V*ca via their buried volume (%V_{Burr}) as proposed by Cavallo and coworkers in a study of L(Cp)Rh motifs with L = NHC,[58] which will be discussed in detail later. The σ-donating and π-accepting abilities of selected CAACs were assessed with the energies of their HOMO and LUMO, using DFT calculations, **Figure 2**. A high-energy HOMO (strong σ-donating character) and a low-lying LUMO (strong π-accepting character) are expected to lead to strong M–C_c bonds in CAAC complexes. The C_α attached to the carbene carbon, changing the two methyl groups to a bulky cyclohexane substituent (**2**) does not change the HOMO-LUMO gap by much (~0.04 eV), and the ΔG_{S-T} increases by ~3 kcal/mol.

To date, synthesis of CAACs requires an aryl group bonded to the nitrogen center.[31] When changing the methyl group on the nitrogen center to an aryl group, diisopropylphenyl (Dipp), the HOMO-LUMO gap increases from 8.42 (**1**) to 8.51 (**3**) eV. Replacement of the alkyl group by an amine group (at the position adjacent to the nitrogen) for CAAC **4** significantly increases the HOMO-LUMO gap from 8.42 to 8.75 eV. Unsaturation on the ring has a noticeable effect on the HOMO-LUMO gap (8.75 eV for **4** vs. 8.29 eV for **5**), indicating stronger σ-donating and the π-accepting ability. According to our MCSCF active space molecular orbital (MO) analysis, this seems to be due to the delocalization of the N–C_c π bonding and antibonding orbitals, **Figure S1**. The HOMO-LUMO gap becomes smaller when the ring size increases from five (**1**) to six (**6**) (8.42 and 8.02 eV, respectively). This destabilization of the carbene lone pair (HOMO) is proposed to be due to the ∠N–C_c–C_α bond angle increase upon going from a five-membered ring to a six-membered ring (from 106.0° to 117.6°), see **Table 1**. The NHC **7** shows a lower HOMO energy level than that of CAAC **1** - **6**, which is expected when a π-donating amino group is replaced by a σ-donating alkyl group. The singlet and triplet free energy gaps for CAAC models are calculated and shown in **Figure 2**. All the DFT-optimized CAACs are predicted to have a stable singlet ground state, as expected. The energy splitting between singlet and triplet for five-membered CAAC (~48 to 50 kcal/mol) is much larger than the six-membered CAAC (~36 kcal/mol). It could indicate that a larger ring size could make triplet states more accessible for the CAAC, perhaps upon ligation to a metal center. The singlet state NHC **7** is 72.1 kcal/mol more stable than the triplet state, which correlates with the increasing electronegativity of the π-donating amino group vs. that of the alkyl group.

1.3. MCSCF Natural Orbital Analysis

Given the challenges for DFT in describing virtual orbitals, it was decided to further investigate the nature of the frontier orbitals of the CAAC ligands by performing multi-configuration self-consistent-field (MCSCF) calculations with the 6-31G(d) basis set on the singlet state of CAACs **1** - **6**, **Figure 2**. Active spaces from (2,2) to (12,12) were analyzed and (8,8) was chosen as representative based on these results. All MCSCF calculations use the complete active space SCF (CASSCF) protocol. Natural orbitals of CAAC ligands are obtained from the MCSCF calculations and the relevant natural orbital occupation numbers (NOONs) computed. The key frontier orbitals of **1** - **6** are shown in **Figure S1**. Full details of the key natural orbitals in the CASSCF active space are given in the Supporting Information. Taken

together, the MCSCF calculations imply that several candidate orbitals are close in energy both at the top of the valence band and the bottom of the conduction band, and the electronic properties of CAAC will thus be very sensitive to both ring size and substituents.

2. CAAC Ligands in C–H Insertion

Highly π-acidic CAAC ligands have been shown to be very reactive as compared to NHC ligands. A computational study by Su and Chu with B3LYP and CCSD methods on NHCs found them to be unreactive towards C–H insertion into methane (barriers > 56 kcal/mol).[59] Turner has shown experimentally that CAAC shielded by a 2,6-diisopropylphenyl (Dipp) substituent on the nitrogen is able to activate the relatively acidic *sp*-, sp^2-, sp^3-hybridized C–H bonds of phenylacetylene, pentafluorobezene and chloroform (pKa = 29, 27 and 16, respectively).[55] Our calculations show that chloroform C–H activation with **1** has an activation barrier of only 10.8 kcal/mol, consistent with the observed reactivity of Turner *et al*.[55] Thus, it was decided to assess whether methane (pKa ~ 50), a smaller, more refractory hydrocarbon, could undergo metal-free C–H activation by CAACs from the computational perspective, given the importance of methane as the major component of natural gas.

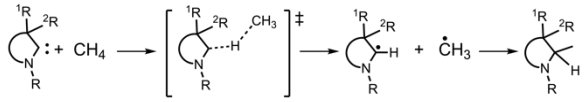

Scheme 1. Homolytic H-atom abstraction (HAA) pathway at C_c of CAACs.

Activation of the methane C–H bond can occur through either homolytic or heterolytic cleavage. Non-concerted C–H insertion transition states for methane are located for CAACs **1** – **6**. Calculations (ωB97XD/6-311++G(d,p)) suggest that methane C–H activation by CAACs goes via an H-atom abstraction (HAA) pathway at C_c, forming a methyl radical, which is followed by a radical rebound to form a new C_c–Me bond, **Scheme 1**. A Mulliken spin density calculation of the open-shell singlet TS shows small radical character developing on the dissociating methyl group, which supports the activation process as a hybrid of both homolytic and heterolytic (~+0.1 - +0.2 in charge with CAAC **1** - **6**). This resembles the hybrid H_2 activation mechanism modelled by Frey *et al.*, which is a step-wise carbene insertion into a H_2 bond whereby H_2 becomes slightly polarized upon activation.[37] The optimization of the singlet and triplet C–H activation TSs yields different geometries, **Figure 3**. The singlet TSs for **1** - **6** show a C_c–H–Me bond angle much smaller than 180˚ (114˚-120˚), while the triplet TSs have a C_c–H–Me close to 180˚ (175˚- 180˚ for **1**, **2**, **4**, **5**, **6** and 160˚ for **3**). This is drastically different from the TS structure of chloroform activation, for which the singlet HAA linear TS (179˚) is 17.5 kcal/mol lower than the isomeric singlet bent TS (118˚), which is expected due to chloroform's high polarity. Triplet HAA TS for chloroform is 40.8 kcal/mol higher in free energy than singlet and the optimized geometry shows a slightly more bent C_c–H–Me bond angle (176˚). According to Mayer *et al.* on the mechanistic distinctions between HAA and proton coupled electron transfer (PCET) mechanisms,[60] the singlet CAAC C–H activation is best described as a three-electron, three-center HAA with mainly a bond stretching vibrational contribution, based on the calculated geometrical parameters. The triplet TSs are better described as PCET with a mix of bending and stretching vibrational characters. For **1**, **2**, **4** and **5**, the singlet TS is favored by 14 - 15 kcal/mol in free energy versus the triplet, while the singlet TS for **3** is favored by 34 kcal/mol. The difference between the singlet and the triplet TS for **6** is only 10 kcal/mol, consistent with the computational evidence given above suggesting that the S and T states of **6** are closer in energy.

The results for different CAACs are similar in terms of reaction free energy barriers ($\Delta G^{\ddagger}$) and exergonicity (ΔG). The calculated C–H activation $\Delta G^{\ddagger}$ are 43.8 (**1**), 43.3 (**2**), 47.7 (**3**), 47.0 (**4**), 50.6 (**5**), 41.6 (**6**), 53.8 (**7**) kcal/mol, respectively, see **Table 2**. The high barriers are likely due to the high pKa of methane, given the low barrier computed for activation of the C_{sp3}–H bond of chloroform, but are interesting in terms of the favourable computed energetics. All CAACs calculated have a lower methane activation barrier than NHC **7**, which agrees with the stronger nucleophilicity of CAACs. The reaction was computed to be highly exergonic. The insertion product is 24.2, 28.1 and 27.7 kcal/mol in free energy below the reactants for **1**, **2** and **3**, respectively, while those for **4**, **5**, and **6** are 28.3, 11.8 and 30.8 kcal/mol, respectively. For NHC **7**, the insertion product is only 8.5 kcal/mol lower in free energy than the reactants. The significant difference in thermodynamics between NHC and CAAC is expected because CAACs are a poor leaving group compared to NHCs due to CAACs' higher basicity. Therefore, CAACs are less suitable for organocatalysis than NHCs for small molecule activation. Compared to **4**, the unsaturation in the ring of **5** seems to make a drastic difference in terms of insertion exergonicity, which is likely due to the high thermodynamic stability of its CAAC reactant. The stability of **5** in its singlet state is demonstrated by its large ΔG_{S-T} (51.3 kcal/mol), which may be due to conjugation from the carbon-carbon double bond. The interaction from the empty carbene p-orbital and the HOMO of the double bond π-orbital thus stabilizes the singlet carbene. But C–H insertion leads to the disruption of this conjugated system, which could destabilize the insertion product. Its relatively high $\Delta G^{\ddagger}$ (50.6 kcal/mol) and singlet stability suggests **5**'s low reactivity of the C_c. Calculations of the bond dissociation free energies (BDFEs) indicate that the C_c–H bond formed in the intermediate for **6** is 3 – 6 kcal/mol stronger than for **1** and **2**, which may also yield a lower barrier for methane activation by **6**.

L	ΔG_{S-T}	ΔG	$\Delta G^{\ddagger}$
1	47.7	-24.2	43.8
2	50.1	-28.1	43.3
3	47.1	-27.7	47.7
4	48.9	-28.3	47.0
5	51.3	-11.8	50.6
6	36.0	-30.8	41.6
7	72.1	-8.5	53.8

Table 2. ΔG_{S-T} is the free energy difference between singlet and triplet of the carbenes **1** - **7**. ΔG is the change is free energy of the C_c insertion into the C–H bond of methane. $\Delta G^{\ddagger}$ is the activation barrier. All free energies are in kcal/mol.

Figure 3. Transition state geometries of C–H activation by CAAC **1** (A) singlet, methane, (B) triplet, methane, (C) singlet, chloroform. Bond lengths and angles in Angstrom units and degrees, respectively.

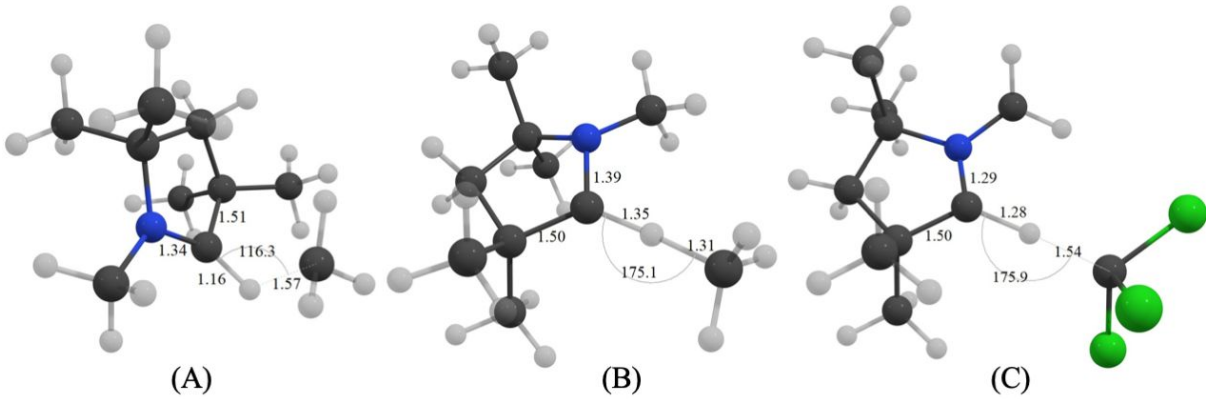

3. L(Cp)M (M = Co, Rh, Ir) for Methane C–H Oxidative Addition

Clement *et al.* have shown that coordinatively unsaturated Pd^0 and Ni^0 complexes supported by a strongly σ-donating NHC ligand is able to activate the C–H bond of an imidazolium salt,[61,62] forming metal hydride complexes, which is very similar to the (NHC)Rh(I) C–H activation by Wiedemann *et al.*[63] It was thus decided to evaluate CAACs, which are even stronger σ-donating ligands than NHCs, for oxidative addition of methane to (CAAC)CpM^I. Methane oxidative addition (OA) to these 16-electron intermediates formally results in an 18-electron product. The papers by Carreón-Macedo *et al.* and Siegbahn and co-workers offer very comprehensive explanations from a computational perspective on methane oxidative addition by (OC)CpM^I.[21,22] We also calculated methane C–H activation with L(Cp)M with L = CO, PMe_3 and M = Co, Rh, Ir (ωB97XD/6-31G(d)//6-311G(d,p)) as a calibration of the functional choice and as a comparison with using CAACs as ancillary ligands where L = **1** - **6**. The present calculations with L = CO and PMe_3 show good agreement with the experimental results from Bergman and Graham and computational data from Siegbahn.[22] CAAC **1** and **6** and NHC **7** were modelled as ancillary ligands for all three metals in preliminary calculations. Rh showed the most interesting results from the preliminary studies and therefore calculations with this metal and CAACs **2** - **5** as ancillary ligands were performed at the same level of theory.

The important geometrical parameters of optimized reactant complexes with CO, PMe_3, **1**, **6** and **7** as ancillary ligands are shown in **Table 3**. The changes in geometries for (OC)CpM and (Me_3P)CpM between the singlets and triplets are very small (less than 0.1 Å for Rh–L and Rh–Z distance and less than 1˚ for ∠L–Rh–Z), which agrees with their similar thermal stability. The changes in key bond lengths and angles between singlets and triplets for L(Cp)Co remain very small, but the changes in ∠L–Rh–Z are slightly larger (1˚ for **1** and 2˚ for **6**). For L(Cp)Rh where L = **1** and **6**, the elongation of Rh–L bond is more significant than that of L = CO and PMe_3 (0.11 Å for **1** and 0.15 Å for **6**) upon going from the singlet to the triplet state. For L(Cp)Ir, the changes in Ir–L and Ir–Z are smaller than 0.1 Å. **1** and **6** show a larger ∠L–M–Z than CO and PMe_3 for all three metals, indicating CAACs have greater steric bulk. NHC **7** shows similar M–L and M–Z distances compared to **1** and **6**. The shorter (~0.3 - 0.4 Å) M–L bond length with CAAC versus that with PMe_3 can benefit catalytic systems that require large steric hindrance, by positioning the ancillary ligands closer to the metal center.

	L	Spin state	ΔG_{S-T} (kcal/mol)	M–L (Å)	M–Z (Å)	∠L–M–Z (˚)
Co	CO	singlet	11.1	1.77	1.78	136.5
		triplet		1.77	1.81	137.5
	$P(Me)_3$	singlet	12.6	2.18	1.77	138.5
		triplet		2.18	1.80	139.1
	1	singlet	13.1	1.87	1.79	148.4
		triplet		1.88	1.86	149.9
	6	singlet	13.1	1.86	1.80	151.9
		triplet		1.88	1.87	153.9
	7	singlet	12.9	1.90	1.79	149.8
		triplet		1.90	1.84	150.9
Rh	CO	singlet	-1.1	1.84	1.92	136.7
		triplet		1.90	1.97	137.1
	$P(Me)_3$	singlet	2.0	2.26	1.94	136.8
		triplet		2.31	1.96	137.5
	1	singlet	-3.8	1.89	1.92	142.0
		triplet		2.08	2.02	177.0
	6	singlet	-11.3	1.88	1.92	146.6
		triplet		2.03	1.98	143.4
	7	singlet	-0.3	1.91	1.92	142.7
		triplet		2.05	1.97	141.4
Ir	CO	singlet	1.5	1.84	1.93	141.3
		triplet		1.86	1.95	140.5
	$P(Me)_3$	singlet	0.6	2.25	1.92	141.1
		triplet		2.27	1.94	140.3
	1	singlet	-5.7	1.89	1.92	146.8
		triplet		1.97	1.97	144.4
	6	singlet	-14.8	1.92	1.90	146.6
		triplet		2.02	1.96	147.3
	7	singlet	-2.0	1.91	1.91	147.4
		triplet		2..00	1.95	144.2

Table 3. ωB97XD/6-311++G(d,p) calculated geometries of reactants L(Cp)M. Z is the centroid of the Cp ligand.

All complexes studied in this work are computed to follow a concerted C–H oxidative addition passage to form the insertion product complex: $L(Cp)M + CH_4 \rightarrow L(Cp)M(H)(CH_3)$. (OC)CpCo has a 19.8 kcal/mol calculated $\Delta G^{\ddagger}$ for methane oxidative addition while (Me_3P)CpCo has a 32.7 kcal/mol free energy barrier. Neither complex has demonstrated the ability to activate hydrocarbons in experiments, which is likely due to the weak Co–H/C bond energies. Calculations from Siegbahn[22] and our group[64] show that a spin crossover is required to go from triplet reactant complex to a singlet oxidative addition product, which further inhibits cobalt-based reactions with methane. We attempted to calculate the binding energy of methane by looking for the σ-complexes ($L(Cp)Co\text{--}CH_4$) with all L studied. But all attempts led either to product or methane dissociation at the level of theory chosen. The high effective nuclear charge and the localized *3d* orbitals of Co make it hard for the reactant precursor σ-complex to form. For M = Rh, calculation shows a barrier height of 5.5 kcal/mol with (OC)CpRh, which is only 1 kcal/mol higher than the experimental value measured by Wasserman *et al.*[11] The free energy barrier to methane activation by (Me_3P)CpRh is calculated to be marginally lower than the carbonyl derivative, 4.9 kcal/mol. Methane activations with (OC)CpIr and (Me_3P)CpIr are calculated to be barrierless, which agrees with computational data reported Siegbahn.[22]

Among three metals, the singlet-triplet splitting varies when different CAACs act as the ancillary ligands. For both L = **1** and **6**, triplet states are favored by 13.1 kcal/mol for L(Cp)Co. These values are very close to the ΔG_{S-T} computed when L = CO (11.1 kcal/mol) and PMe_3 (12.6 kcal/mol). For L = **7**, triplet state is favored by 12.9 kcal/mol. For L(Cp)Ir, **1**, **6** and **7** stabilize a singlet ground state of the metal complex with ΔG_{S-T} = -5.7, -14.8 and -2.0 kcal/mol for L = **1**, **6** and **7**, respectively. The (CAAC)(Cp)Rh complexes have varied singlet-triplet splitting patterns: 3.8 (**1**), 4.8 (**2**), 6.7 (**3**), 4.1 (**4**), 0.2 (**5**), 11.3 (**6**), 0.3 (**7**) kcal/mol in favor of the singlet. The donor ability and the field strength of CAAC ligands are highly tunable by adjusting the steric and the electronic properties from the substituents on the C_α and amino group. Compared to CAACs **1** - **5**, **6** does a better job stabilizing the singlet state despite the Rh atom's low excitation energy (7.8 kcal/mol) from ground state d^8s^1 to the excited state d^9.[22] Both L(Cp)Ir and L(Cp)Rh show singlet-triplet near-degeneracy when NHC **7** is the ancillary ligand with singlet state being slightly favored by 0.3 and 2.0 kcal/mol for Rh and Ir, respectively. Mulliken population analyses with unrestricted DFT methods on singlet states indicate that L(Cp)M supported by CAAC ligands have much lower spin densities than when L = CO, PMe_3 and NHC **7**, which could be due to the stronger donor ability of CAAC ligands than that of PMe_3 and CO ligands. MCSCF calculations were performed on L(Cp)M with L = **1** and **6** for all three metals to study the bonding in transition metal carbene complexes. CAS(12,12) active space was used after experimenting with several active space sizes and initial wavefunction guesses. MCSCF calculated natural orbitals show the M–C_c bond in both singlet and triplet state consists of a relatively covalent σ bond and one very polarized π bond. The NO plot and occupation numbers of natural orbital and occupancies of metal and carbene carbon are shown in SI. Triplet states of all three metals are predominantly metal-based triplets with the unpaired electron resides on the nonbonding *d* orbitals. The two singly occupied natural orbitals of three metals all have 1 e^- total occupancy: 0.95 and 0.93 e^- for Co, 0.81 and 0.80 e^- for Rh, 0.90 and 0.79 e^- for Ir. Frontier molecular orbitals of the L(Cp)Ir and L(Cp)Rh motifs suggest

that the strong σ-donating strength of **1** and **6** destabilizes the d_{σ}. We propose based on the current results, that CAACs are better donors than NHC **7** and PMe_3 and offer easier access to the low spin ground state for L(Cp)Rh and L(Cp)Ir. However, the differences in donor ability seem to have little effect on L(Cp)Co, which might be due to the Co's high nuclear charge and the highly-stabilized near-degenerate *d* orbitals.[13]

For methane activation with L(Cp)M with CAACs as ancillary ligands, the relative energies of transition states and of oxidative addition products with respect to the reactants, L(Cp)M + CH_4, are shown in **Table 4**. Free energy profiles with both singlet and triplet surface in methane activation are shown in **Figure** S7 to S15. **1**(Cp)Co, **6**(Cp)Co and **7**(Cp)Co have 38.1, 42.1 and 36.3 kcal/mol free energy barriers, respectively. This might be due to the poor ability of the triplet states of the cobalt carbene complexes to bind methane. Oxidative addition of methane to **1**CpCo is less endergonic than L = CO and $P(Me)_3$, ΔG = 4.9 kcal/mol. The OA product of methane oxidative addition to **6**(Cp)Co is 36.5 kcal/mol uphill as compared to reactants. The triplet state **1**(Cp)Co(H)(CH_3) is favored by 25.9 kcal/mol, while the singlet state is favored for L(Cp)Co(H)(CH_3) when L = CO, PMe_3 and **6**.

`	L	ΔG_{S-T} of L(Cp)M	$\Delta G^{\ddagger}$	ΔG
Co	CO	12.6	19.8	14.7
	$P(Me)_3$	11.1	32.7	23.6
	1	13.1	38.1	4.9
	6	13.1	42.1	36.5
	7	12.9	36.3	25.2
Rh	CO	-1.1	5.5	-3.5
	$P(Me)_3$	2.0	4.9	-8.5
	1	-3.8	12.2	1.2
	6	-11.3	20.2	11.6
	7	-0.3	8.0	-5.2
Ir	CO	0.6	-6.8	-27.6
	$P(Me)_3$	1.5	-3.2	-30.7
	1	-5.7	7.1	-16.2
	6	-14.8	36.1	-4.1
	7	-2.0	5.0	-24.3

Table 4. ωB97XD/6-311++G(d,p) calculated singlet-triplet free energy splitting of L(Cp)M, relative energies of the TSs ($\Delta G^{\ddagger}$) and of OA products (ΔG) with respect to the reactants, L(Cp)M + CH_4. Only the relative energies of the most stable OA TS and OA product spin states are shown.

Compared to L = CO and $P(Me)_3$, methane C–H activation with L(Cp)Ir when L = **1** or **6** is much less exergonic as well: -30.7 kcal/mol for PMe_3 and -27.6 kcal/mol for CO vs. -16.2 kcal/mol for **1** and -4.1 kcal/mol for **6**. Both (OC)(Cp)Ir and (Me_3P)(Cp)Ir are calculated to have a negative free energy barriers of -6.8 and -3.2 kcal/mol, which is close to the -1.8 kcal/mol from Siegbahn's work on (OC)(Cp)Ir.[22] There is a chance that the negative barriers arise from basis set effects. Houk *et al.* argued that unfavourable entropic factors could lead to negative values of $\Delta S^{\ddagger}$; methane additions are so exothermic that enthalpy decreased all along the reaction profile.[65] But for L = **1** and **6**, the barriers for C–H activation are 7.1 and 36.1 kcal/mol, respectively. The higher barrier reflects the higher thermodynamic stability of the singlet reactant complex. Both **1**(Cp)Rh and **6**(Cp)Rh shows very reasonable activation barriers of 12.2 and 20.2 kcal/mol, respectively, although methane OA is endergonic for both: 1.2 and 11.6 kcal/mol higher than their respective reactants. NHC **7** appears to be the middle ground between CAAC **1** and PMe_3 in terms of OA kinetics and thermodynamics, **Table 4**.

Based on the reasonable methane activation barriers calculated for **1**(Cp)Rh and **6**(Cp)Rh, it was decided to model the remaining CAACs (**2** - **5**) as supporting ligands for (Cp)Rh. Calculated binding free energy of CO, PMe_3 and **1** - **6** to Rh in LCpRh is shown in **Table 5**. The CAAC ligands have a stronger binding to Rh than CO by 11 - 21 kcal/mol and stronger than PMe_3 by 15 - 25 kcal/mol. Although it may be expected that a high-lying HOMO (strong donor) and a low-lying LUMO (strong π-acceptor) lead to stronger ligand-metal bonding, this does not appear to be the case in the present calculations. Based on our data for the HOMO-LUMO gap of the free ligands and their binding free energies to Rh, the ligand binding ΔG is not directly correlated to its HOMO and LUMO energy levels. For example, **3** shows a 0.01 eV higher LUMO and 0.08 eV lower HOMO than **1**, but **3** binds 2.2 kcal/mol more strongly than **1** to Rh. **5** has a lower LUMO and higher HOMO than **1**, but it binds 7.4 kcal/mol more strongly than **1**. In terms of the impact of a bulky cyclohexyl substituent on CAAC, the binding energy of **2** is 5.4 kcal/mol lower than **1**. Considering they have very close HOMO and LUMO energy levels, steric factors seem to be dominant here.

CAACs generally better stabilize the singlet state of L(Cp)Rh than CO or PMe_3, except **5**. But **6**(Cp)Rh seems to suggest that the stabilization of the singlet seems has a very small impact on the activation barrier, which is quite surprising considering singlet reactant complexes have shown better performance in forming the reactant σ-complex precursor.[38] Buried volumes ($\%V_{Bur}$) were also calculated for CAACs and PMe_3 at the DFT-optimized geometries to quantify steric profile. $\%V_{Bur}$ is a lot larger for CAACs with bulky cyclohexane (**2**) and aromatic (**3**) substituents than the parent CAAC (**1**). Surprisingly, the two diamino-CAACs with saturated (**4**) and unsaturated (**5**) backbones have $\%V_{Bur}$ values close to that of **2** with bulky cyclohexane substituent on C_{α}. **6** shows that bigger ring size will increase the $\%V_{Bur}$ by ~24%. Overall, buried volume calculations show that CAAC ligands have very tunable steric properties by introducing different substitutions on the C_{α} and N_{α} as well as adjusting the ligand ring size. Buried volumes have been shown to vary based on metal center itself and metal-ligand bond length, especially certain ligands are more influenced by the metal and its environment than the others.

L	ΔG_{S-T} of L(Cp)Rh	binding ΔG	$\Delta G^{\ddagger}$	ΔG	$\%V_{Bur}$
CO	-1.1	45.1	5.6	-3.4	N/A
PMe_3	2.0	40.4	4.9	-8.2	48.9
1	-3.8	62.3	12.2	1.2	30.8
2	-4.8	56.9	11.8	-0.8	53.7
3	-6.7	64.5	27.1	18.6	61.6
4	-4.1	59.8	11.1	-0.8	53.5
5	-0.2	54.9	13.1	-5.4	51.1
6	-11.3	65.9	20.2	11.6	54.3

Table 5. Energy profile of singlet L(Cp)Rh catalyzed OA with methane. All the energies are in kcal/mol. Buried volume ($\%V_{Bur}$) values for PMe_3 and CAAC ligands are shown.

Summary and Conclusions

This project provides insight into the selection of CAAC supporting ligands for organometallic C–H activation. Three main parts of this study include (1) evaluating the electronic properties and structures of the selected cyclic alkyl(amino) carbene (CAAC) ligands, (2) analyzing C–H insertion into methane by isolated CAACs, and (3) studying CAACs as ancillary ligands in (CAAC)(Cp)M (M = Co, Rh, Ir) transition metal complexes and their ability to effect methane C–H oxidative addition in comparison to (Me_3P)(Cp)M and (OC)(Cp)M. The main conclusions are summarized below.

(1) Both DFT and MCSCF calculations show that CAAC ligands have highly tunable donor and acceptor ability by modifying the different substituents on the amino group and the alpha carbon as well as the cyclic backbone, which could make this group of ligands very versatile in homogeneous catalysis. But due to CAACs' unusual electronic structures and the limitation of DFT in describing frontier orbitals, particularly virtual orbitals, can make it difficult to accurately model the electronic structures of this class of organic compounds using only DFT. MCSCF calculations in particular reveal that the frontier orbitals of the CAAC ligands are very sensitive to the substituents and the ring size. The calculated electron density plot of the six-membered rings CAAC **6** shows more substantial delocalization than those of the five-membered ring CAACs **1** - **5**, which may impact the back-bonding properties when functioning as a

ligand as compared to five-membered ring CAACs. The unsaturated backbone of **5** causes delocalization of the N–C_c π bonding and antibonding orbitals as well.

(2) Calculations of C–H activation of chloroform by CAAC **1** are consistent with the experimental observations from the Turner group,[40] supporting the validity of the chosen computational methods. Barriers for C–H activation of methane by CAAC ligands are, *ca.* 40 to 50 kcal/mol, which is much higher than the 10.8 kcal/mol for chloroform. This is ascribed to the much higher pKa for methane than chloroform (50 vs. 16), given the latter has a stronger homolytic bond energy than methane, suggesting a transition state for activation that has a surprising degree of PCET character. Methane activation with NHC **7** is calculated to be much less endergonic than with CAACs, which is expected due to CAACs' higher basicity. CAAC singlet state stability and the thermodynamic stability of the product and radical intermediate could all play a role in the CAAC's reactivity towards C-H bond activation. Our computational data suggests that the diamino CAAC with unsaturated ring (**5**) has the potential of destabilizing the methane activation product when the conjugation is disrupted in the reaction, which could be useful in small-molecule catalysis.

(3) When acting as an ancillary ligand for Group 9 metals, CASSCF results showed that the metal-carbene bond consists of a relatively covalent σ bond and one very polarized π bond for both singlet and triplet states. CAAC **1** and **6** showed very different behaviour in stabilizing the ground states of L(Cp)M (M = Co, Rh, Ir) compared to CO and PMe_3. We believe both metal effects and ligand can have an impact on stabilizing singlet Cp-based group 9 metal catalysts, while ligand effects can be much stronger for Rh and Ir. For lighter transition metals like cobalt, the much stronger donor ability of CAAC has limited impact upon stabilizing the singlet state of the reactive complex. When L = **1** and **6**, L(Cp)Rh and L(Cp)Ir show a large energetic preference for the singlet state versus the near degeneracy of singlet and triplet states when L = CO and PMe_3, which may be due to the strong σ-donor ability of the CAAC class ligands. NHC **7** seems be the middle ground between PMe_3 and CAAC **1** in terms of singlet stability and the reaction energetics. With NHC and CAAC ancillary ligands, L(Cp)Rh and L(Cp)Ir reactions show higher barriers and higher exergonicity, which could potentially render the reaction more catalytic than stoichiometric. But the challenge to quantify the relationship between the ligand donor-acceptor properties vs. the reaction thermodynamics and/or kinetics remains in studying organometallic catalysis.

Our computational data of CAAC **1** - **6** within the L(Cp)Rh motif suggest that this class of cyclic carbene ligand does not fit into the classic Fischer or Schrock carbene ligand category. The electronic and the steric characteristics of CAACs can potentially be tuned for different applications by changing the substituents and the backbone. From the buried volume (%V_{Bur}) calculations for L(Cp)Rh motifs, the CAACs show very tunable steric properties as well by adjusting the ring-size and the substituents on the C_α (%V_{Bur} ~ 30.8 - 61.6). But the stability of the singlet L(Cp)Rh depends more on the stability of the CAAC ligand singlet ($\Delta G_{S\text{-}T}$ of CAACs), while steric differences play a smaller role. So far, CAACs have shown great potential in stabilizing low-valent metal complexes due to CAACs' strong *π*-acidity. But more experimental and computational studies are needed to better understand the electronic structure of the CAAC metal complexes.

Conflicts of interest

There are no conflicts to declare.

Acknowledgements

We thank the NSF for their support of this work via grants CHE-1464943 and CHE-1531468, the latter funding the purchase of the UNT Dept. of Chemistry high-performance computing cluster.

Reference

(1) Crabtree, R. H. Organometallic alkane CH activation. *J. Organomet. Chem.* **2004**, 689, 4083-4091.
(2) Shul'pin, G. B. C–H functionalization: thoroughly tuning ligands at a metal ion, a chemist can greatly enhance catalyst's activity and selectivity. *Dalton Trans.* **2013**, *42*, 12794-12818.
(3) Jazzar, R.; Hitce, J.; Renaudat, A.; Sofack-Kreutzer, J.; Baudoin, O. Functionalization of organic molecules by transition-metal-catalyzed $C(sp^3)$–H activation. *Chem. Eur. J.* **2010**, 16, 2654-2672.
(4) Balcells, D.; Clot, E.; Eisenstein, O. C–H bond activation in transition metal species from a computational perspective. *Chem. Rev.* **2010**, 110, 749-823.
(5) Xue, X. S.; Ji, P.; Zhou, B.; Cheng, J. P. The essential role of bond energetics in C–H activation/functionalization. *Chem. Rev.* **2017**, 117, 8622-8648.
(6) Qin, Y.; Zhu, L.; Luo, S. Organocatalysis in inert C–H bond functionalization. *Chem. Rev.* **2017**, 117, 9433-9520.
(7) Niu, S.; Hall, M. B. Theoretical studies on reactions of transition-metal complexes. *Chem. Rev.* **2000**, 100, 353-406.
(8) Gunsalus, N. J.; Koppaka, A.; Park, S. H.; Bischof, S. M.; Hashiguchi, B. G.; Periana, R. A. Homogeneous functionalization of methane. *Chem. Rev.* **2017**, 117, 8521-8573.
(9) Janowicz, A. H.; Bergman, R. G. C–H activation in completely saturated hydrocarbons: direct observation of M + R–H → M(R)(H). *J. Am. Chem. Soc.* **1982**, 104, 352-354.
(10) Janowicz, A. H.; Bergman, R. G. Activation of C–H bonds in saturated hydrocarbons on photolysis of $(\eta^5\text{-}C_5Me_5)(PMe_3)IrH_2$. relative rates of reaction of the intermediate with different types of C–H bonds and functionalization of the metal-bound alkyl groups. *J. Am. Chem. Soc.* **1983**, 105, 3929-3939.
(11) Wasserman, E. P.; Moore, C. B.; Bergman, R. G. Gas-phase rates of alkane C–H oxidative addition to a transient CpRh(CO) complex. *Science*. **1992**, 255, 315-318.
(12) Schultz, R. H.; Bengali, A. A.; Tauber, M. J.; Weiller, B. H.; Wasserman, E. P.; Kyle, K. R.; Moore, C. B.; Bergman, R. G. IR flash kinetic spectroscopy of C–H bond activation of cyclohexane-d_0 and -d_{12} by $Cp^*Rh(CO)_2$ in liquid rare gases: kinetics, thermodynamics, and unusual isotope effect. *J. Am. Chem. Soc.* **1994**, 116, 7369.
(13) Bengali, A. A.; Bergman, R. G.; Moore, C. B. Evidence for the formation of free 16-electron species rather than solvate complexes in the ultraviolet irradiation of $CpCo(CO)_2$ in liquefied noble gas solvents. *J. Am. Chem. Soc.* **1995**, 117, 3879-3880.
(14) Jones, W. D.; Feher, F. J. Comparative reactivities of hydrocarbon carbon-hydrogen bonds with a transition-metal complex. *Acc. Chem. Res.* **1989**, 22, 91-100.
(15) Jones, W. D.; Feher, F. J. The mechanism and thermodynamics of alkane and arene carbon-hydrogen bond activation in $(C_5Me_5)Rh(PMe_3)(R)H$. *J. Am. Chem. Soc.* **1984**, 106, 1650-1663.
(16) Jones, W. D.; Feher, F. J. Mechanism of arene carbon-hydrogen bond activation by $(C_5Me_5)Rh(PMe_3)(H)Ph$. Evidence for arene precoordination. *J. Am. Chem. Soc.* **1982**, 104, 4240-4242.
(17) Hoyano, J. K.; McMaster, A. D.; Graham, W. A. G. Apliphatic hydroxylation catalyzed by iron porphyrin complexes. *J. Am. Chem. Soc.* **1983**, 105, 7190-7191.
(18) Hoyano, J. K.; Graham, W. A. G. Oxidative addition of the carbon-hydrogen bonds of neopentane and cyclohexane to a photochemically generated iridium(I) complex. *J. Am. Chem. Soc.* **1982**, 104, 3723-3725.
(19) Ziegler, T.; Tschinke, V.; Fan, V.-Y.; Becke, A. D. Theoretical study on the electronic and molecular structures of $(C_5H_5)M(L)$ (M = Rh, Ir; L= CO, PH_3) and $M(CO)_4$ (M = Ru, Os) and their ability to activate the C–H bond in methane. *J. Am. Chem. Soc.* **1989**, 111, 9177.
(20) Musaev, D. G.; Morokuma, K. Ab initio molecular orbital study of the mechanism of H–H, C–H, N–H, O–H and Si–H bond activation on transient cyclopentadienylcarbonylrhodium. *J. Am. Chem. Soc.* **1995**, 117, 799-805.
(21) Carreón-Macedo, J.; Harvey, J. N. Do spin state changes matter in organometallic chemistry? A computational study. *J. Am. Chem. Soc.* **2004**, 126, 5789-5797.
(22) Siegbahn, P. E. M. Comparison of the C−H activation of methane by $M(C_5H_5)(CO)$ for M = cobalt, rhodium, and iridium. *J. Am. Chem. Soc.* **1996**, 118, 1487-1496.
(23) Igau, A.; Grutzmacher, H.; Baceiredo, A.; Bertrand, G. Analogous α,α'-bis-carbenoid triply bonded species: synthesis of a stable λ^3-phosphinocarbene-λ^5-phosphaacetylene. *J. Am. Chem. Soc.* **1988**, 110, 6463-6466.
(24) Arduengo III, A. J.; Harlow, R. L.; Kline, M. A stable crystalline carbene. *J. Am. Chem. Soc.* **1991**, 113, 361-363.
(25) Herrmann, W. A. N-heterocyclic carbenes: a new concept in organometallic catalysis. *Angew. Chem. Int. Ed.* **2002**, 41, 1290-1309.
(26) Crudden, C. M.; Allen, D. P. Stability and reactivity of N-heterocyclic carbene complexes. *Coord. Chem. Rev.* **2004**, 248, 2247-2273.

(27) Doddi, A.; Peters, M.; Tamm, M. N-heterocyclic carbene adducts of main group elements and their use as ligands in transition metal chemistry. *Chem. Rev.* **2019**, 119, 6994-7112.
(28) Burling, S.; Paine, B. M.; Nama, D.; Brown, V. S.; Mahon, M. F.; Prior, T. J.; Pregosin, P. S.; Whittlesey, M. K; Williams, J. M. C−H activation reactions of ruthenium N-heterocyclic carbene complexes: application in a catalytic tandem reaction involving C−C bond formation from alcohols. *J. Am. Chem. Soc.* **2007**, 129, 1987-1995.
(29) Gaillard, S.; Cazin, C. S. J.; Nolan, S. P. N-heterocyclic carbene gold(I) and copper(I) complexes in C–H bond activation. *Acc. Chem. Res.* **2012**, 45, 778-787.
(30) Lavallo, V.; Canac, Y.; Prasang, C.; Donnadieu, B.; Bertrand, G. Stable cyclic (alkyl)(amino)carbenes as rigid or flexible, bulky, electron-rich ligands for transition-metal catalysts: a quaternary carbon atom makes the difference. *Angew. Chem. Int. Ed.* **2005**, 44, 5705-5709.
(31) Bertrand, G.; Sioleilhavoup, M.; Melaimi, M.; Jazzar, R. Cyclic (alkyl)(amino) carbenes (CAACs): recent developments. *Angew. Chem. Int. Ed.* **2017**, 56, 10046-10068.
(32) Munz, D. Pushing electrons−which carbene ligand for which application? *Organometallics*. **2018**, 37, 275-289.
(33) Cundari, T. R. Calculation of a methane C–H oxidative addition trajectory: comparison to experiment and methane activation by high-valent complexes. *J. Am. Chem. Soc.* **1994**, 116, 340-347.
(34) Crabtree, R. H. Transition metal complexation of σ bonds. *Angew. Chem., Int. Ed. Engl.*, **1993**, *32*, 789.
(35) Martin, D.; Soleilhavoup, M.; Bertrand, G. Stable singlet carbenes as mimics for transition metal centers. *Chem. Sci.* **2011**, *2*, 389-399.
(36) Bharadwaz, P.; Dewhurst, R. D.; Phukan, A. K. Metal-free activation of enthalpically strong bonds: unravelling the potential of hitherto unexplored singlet carbenes. *Adv. Syn. Catal.* **2018**, *360*, 4543-4561.
(37) Frey, G. D.; Lavallo, V.; Donnadieu, B.; Schoeller, W. W.; Bertrand, G. Facile splitting of hydrogen and ammonia by nucleophilic activation at a single carbon center. *Science*, **2007**, *316*, 439-441.
(38) Frey, G. D.; Masuda, J. D.; Donnadieu, B.; Bertrand, G. Activation of Si–H, B–H, and P–H Bonds at a single nonmetal center. *Angew. Chem. Int. Ed.* **2010**, 49, 9444-9447.
(39) Würtemberger-Pietsch, S.; Schneider, H.; Marder, T. B.; Radius, U. Adduct formation, B−H activation and ring expansion at room temperature from reactions of HBcat with NHCs. *Chem. Eur. J.* **2016**, *22*, 13032-13036.
(40) Mohapatra, C.; Samuel, P. P.; Li, B.; Niepötter, B.; Schürmann, C. J., Herbst-Irmer, R., Stalke, D.; Maity, B.; Koley, D.; Roesky, H. W. Insertion of cyclic alkyl(amino) carbene into the Si–H bonds of hydrochlorosilanes. *Inorg. Chem.* **2016**, *55*, 1953-1955.
(41) Nelson, D. J.; Nolan, S. P. Quantifying and understanding the electronic properties of N-heterocyclic carbenes. *Chem. Soc. Rev.* **2013**, *42*, 6723-6753.
(42) Huynh, H. V. Electronic properties of N-heterocyclic carbenes and their experimental determination. *Chem. Rev.* **2018**, 118, 9457-9492.
(43) Gusev, D. G. Electronic and steric parameters of 76 N-heterocyclic carbenes in $Ni(CO)_3(NHC)$. *Organometallics*, **2009**, 28, 6458-6461.
(44) Oziminski, W. P.; Ramsden, C. A. Quantitative index of the relative ease of formation and σ-bonding strength of N-heterocyclic carbenes. *J. Org. Chem.* **2016**, 81, 10295-10301.
(45) Oziminski, W. P.; Ramsden, C. A. The influence of substituent field and resonance effects on the ease of N-heterocyclic carbene formation from imidazolium rings. *RSC Adv.* **2018**, 8, 14833-14837.
(46) Clavier, H.; Nolan, S. P. Percent buried volume for phosphine and N-heterocyclic carbene ligands: steric properties in organometallic chemistry. *Chem. Comm.* **2010**, 46, 841-861.
(47) Scholl, M.; Ding, S.; Lee, C. W.; Grubbs, R. H. Synthesis and activity of a new generation of ruthenium-based olefin metathesis catalysts coordinated with 1,3-dimesityl-4,5-dihydroimidazol-2-ylidene ligands. *Org. Lett.* **1999**, 1, 953-956.
(48) Furstner, A.; Ackermann, L.; Gabor, B.; Goddard, R.; Lehmann, C. W.; Mynott, R.; Stelzer, F.; Thiel, O. R. Comparative investigation of ruthenium-based metathesis catalysts bearing N-heterocyclic carbene (NHC) ligands. *Chem. Eur. J.* **2001**, 7, 3236-3253.
(49) Albert, C.; Chen, P. Mechanism and activity of ruthenium olefin metathesis catalysts: the role of ligands and substrates from a theoretical perspective. *J. Am. Chem. Soc.* **2004**, 126, 3496-3510.
(50) Cavallo, L. Mechanism of ruthenium-catalyzed olefin metathesis reactions from a theoretical perspective. *J. Am. Chem. Soc.* **2001**, 124, 8965-8973.
(51) Frisch, M. J. et al. *Gaussian 16*, Revision C.01, Gaussian, Inc., Wallingford CT, **2016**.
(52) Chai, J. D.; Gordon, M. H. Long-range corrected hybrid density functionals with damped atom–atom dispersion corrections. *Phys. Chem. Chem. Phys.* **2008**, 10, 6615-6620.
(53) Weigend, F.; Ahlrichs, R. Balanced basis sets of split valence, triple zeta valence and quadruple zeta valence quality for H to Rn: Design and assessment of accuracy. *Phys. Chem. Chem. Phys.* **2005**, 7, 3297-3305.
(54) Schmidt, M. W.; Baldridge, K. K.; Boatz, J. A.; Elbert, S. T.; Gordon, M. S.; Jensen, J. H.; Koseki, S.; Matsunaga, N.; Nguyen, K. A.; Su, S.; Windus, T. L. General atomic and molecular electronic structure system. *J. Comp. Chem.* **1993**, *14*, 1347-1363.
(55) Turner, Z. R. Chemically non-innocent cyclic (alkyl)(amino)carbenes: ligand rearrangement, C−H and C−F bond activation. *Chem. Eur. J.* **2016**, *22*, 11461-11468.
(56) Bharadwaz, P.; Chetia, P.; Phukan, A. K. Electronic and ligand properties of skeletally substituted cyclic (alkyl)(amino)carbenes (CAACs) and their reactivity towards small molecule activation: a theoretical study. *Chem. Eur. J.* **2017**, 23, 9926-9936.
(57) Weinstein, C. M.; Junor, G. P.; Tolentino, D. R.; Jazzar, R.; Melaimi, M.; Bertrand, G. Highly ambiphilic room temperature stable six-membered cyclic (alkyl)(amino) carbenes. *J. Am. Chem. Soc.* **2018**, 140, 9255-9260.
(58) Poater, A.; Cosenza, B.; Correa, A.; Giudice, S.; Ragone, F.; Scarano, V.; Cavallo, L. SambVca: A web application for the calculation of the buried volume of N-heterocyclic carbene ligands. *Euro. J. Inorg. Chem.* **2009**, 13, 1759-1766.
(59) Su, M.; Chu, S. Theoretical study of reactions of Arduengo-type carbene, silylene, and germylene with CH_4. *Inorg. Chem.* **1999**, *38*, 4819-4823.
(60) Mayer, J. M.; Hrovat, D. A.; Thomas, J. L.; Borden, W. T. Proton-coupled electron transfer versus hydrogen atom transfer in benzyl/toluene, methoxyl/methanol, and phenoxyl/phenol self-exchange reactions. *J. Am. Chem. Soc.* **2002**, 124, 11142-11147.
(61) Clement, N. D.; Cavell, K. J. Transition-metal-catalyzed reactions involving imidazolium salt/N-heterocyclic carbene couples as substrates. *Angew. Chem., Int. Ed.* **2004**, 43, 3845.
(62) Clement, N. D.; Cavell, K. J.; Jones, C.; Elsevier, C. J. Oxidative addition of imidazolium salts to Ni^0 and Pd^0: synthesis and structural characterization of unusually stable metal–hydride complexes. *Angew. Chem., Int. Ed.* **2004**, 116, 1297-1299.
(63) Wiedemann, S. H.; Lewis, J. C.; Ellman, J. A.; Bergman, R. G. Experimental and computational studies on the mechanism of N-heterocycle C−H activation by Rh(I). *J. Am. Chem. Soc.* **2006**, 128, 2452-2462.
(64) Bellows, S. R.; Cundari, T. R.; Holland, P. L. Spin crossover during β-hydride elimination in high-spin iron(II)–and cobalt(II)–alkyl complexes. *Organometallic*s **2013**, 32, 4741-4751.
(65) Houk, K. N.; Rondan, N. G. Origin of negative activation energies and entropy control of halocarbene cycloadditions and related fast reactions. *J. Am. Chem. Soc.* **1984**, 106, 4293-4294.